ABSORPTION OF METHYL ORANGE USING TITANIA-ALUMINA-GRAPHENE NANOCOMPOSITE BY HYDROTHERMAL SYNTHESIS

by

SITI NURHUDA BINTI MOHD NOR

A thesis submitted in fulfillment of the requirements for the degree of Bachelor of Applied Science (Materials Technology) with Honours

FACULTY OF EARTH SCIENCE
UNIVERSITI MALAYSIA KELANTAN

2017

DECLARATION

I declare that this thesis entitle "Absorption of Methyl Orange Using Titania-Alumina-Graphene Nanocomposite by Hydrothermal Synthesis" is the result of my own research except as cited in the references. The thesis has not been accepted for any degree and is not concurrently submitted in candidature of any other degree.

Signature : _____

Name : _____

Date : _____

ACKNOWLEDGEMENTS

I would like to express my deepest and truthful thanks my supervisor, Dr Mahani Binti Yusoff who expertly guide me through my study since in the beginning until finish. Thank you for always keep understanding, generous and expert guidance that support me which always keep an eye on progress of my works. It was a pleasure working with her, and I also grateful to my co-supervisor Dr Nik Raihan Binti Nik Yusoff.

I would like also to acknowledge and appreciate the laboratory staff of Faculty of Earth Science especially for Mr Rohanif and others lab assistants who always there for me when I need their help in handling machine that I had been used during this study. Thank you for your patience taught and guiding me. Also a lot of thankful for Mr Khairi for his kindness for help in XRD analysis.

I also wish to extend my deepest acknowledgement to my family, without your help I would not be where and who I am today. Particularly for my father and mother, who have patiently supported me throughout my life and helped me out with anything that I have ever needed help with. The immense love and moral support they have given is truly unmeasurable.

Lastly, and most of all it would be really unfair without the mention of my fellow friends which also help me during my study and give me a fun learning environment.

Absorption of Methyl Orange Using Titania-Alumina-Graphene Nanocomposite by Hydrothermal Synthesis

ABSTRACT

In this study, the absorbance of the methyl orange (MO) using TiO_2-Al_2O_3-graphene was synthesized via hydrothermal treatment. The nanocomposite were prepared with different content of TiO_2, Al_2O_3 and graphene. The nanocomposite powder mixture was subjected to hydrothermal treatment at temperature 200°C for 24 h. The morphology, phase identification, crystallite size and functional group were studied using optical microscope, X-ray diffraction and Fourier transform infrared pectrometer. The result showed no new phase formed after hydrothermal synthesized. The nanocomposite of composition 70 wt% TiO_2, 20 wt% Al_2O_3 and 10 wt% graphene showed the lowest crystallite size (26.64 nm). The functional group obtained from the nanocomposite were O-H, N-H and inorganic carbonate group. The composition of without graphene indicate the highest absorbance 32.38% and followed by composition of 50 wt% TiO_2, Al_2O_3 30 wt% and 20 wt% graphene (29.8%) absorbance in visible light.

Penyerapan Metil Oren menggunakan Titania-Alumina-Grafin Nanokomposit oleh Sintesis Hidrotermal

ABSTRAK

Dalam kajian ini, penyerapan metil oren (MO) menggunakan TiO_2 dicampurkan dengan Al_2O_3 dan grafin telah disintesis melalui rawatan hidrotermal. Serbuk nanokomposit telah disediakan dengan kandungan TiO_2, Al_2O_3 dan grafin yang berbeza. Campuran serbuk komposit adalah tertakluk kepada rawatan hidrotermal pada suhu 200°C selama 24 jam. Morfologi, pengenalan fasa, saiz kumin hablur dan kumpulan berfungsi telah dikaji dengan menggunakan mikroskop optik, X-ray pembelauan dan jelmaan Fourier inframerah spektrometer. Hasil menunjukkan tiada fasa baru dibentuk selepas hidroterma disintesis. Komposisi nanokomposit 70 wt% TiO_2, 20 wt% Al_2O_3 dan 10 wt% grafin menunjukkan saiz kumin hablur paling rendah (26.64 nm). Kumpulan berfungsi diperolehi daripada nanokomposit adalah O-H, N-H dan kumpulan karbonat bukan organik. Komposisi tanpa grafin menunjukkan kadar penyerapan tertinggi 32.38% dan diikuti oleh komposisi 50 wt% TiO_2, 30 wt% Al_2O_3 dan 20 wt% grafin (29.8%) di dalam sinaran cahaya.

TABLE OF CONTENT

LIST OF TABLES

LIST OF FIGURES

LIST OF ABBREVIATIONS

CB	Conduction band
CR	Congo red
FTIR	Fourier transform infrared
FWHM	Full width at half maximum
MB	Methylene blue
MC	Mesoporous band
MO	Methyl orange
OM	Optical microscope
SEM	Scanning electron microscope
TEM	Transmission electron microscope
UV	Ultra-violet
UV-Vis	Ultraviolet-Visible spectrophotometer
VB	Valence band
WH	Williamson-Hall method
XRD	X-ray diffraction

LIST OF SYMBOLS

B_r	Overall broadening
C	Concentration
C_o	Initial concentration
D	Intercept of the graph
d	Unit cell
Eg	Energy band gap
k	Constant
n	Internal strain
wt%	Weight percentage
ƛ	Radiation wavelength
Ø	Half of position 2 theta

CHAPTER 1

INTRODUCTION

1.1 Background of Study

Titanium oxide (TiO_2) is one of the n-type semiconductor with a wide gap (3.2 eV) and mostly used as photocatalyst for the oxidative degradation of organic compounds including dyes. Besides, TiO_2 is stable, harmless and inexpensive (Chen *et al*., 2011) which also has excellent properties such as high efficiency of photo-generated electron, chemical inertness, photo-corrosion and chemical corrosion (Mainya *et al*., 2015). TiO_2 photocatalyst was widely used in sterilization, sanitation and remediation applications. It's also used in organic dye photocatalytic and water splitting reaction (Jr *et al*., 2015). In water purification of dye such as degradation of methyl orange (MO), TiO_2 particles serve as catalyst for redox reaction when reactants are absorbed and leading to formation of radicals. These radicals convert organic compounds in dyes to CO_2 and H_2O through oxidation or mineralization process. However, pure TiO_2 has limitation that only active under ultraviolet (UV) region leading slow degradation of the dyes.

Thus, in order to make TiO_2 effective under visible light or lowering the band gap, it can be doped with impurities. Research that have been study by Jr *et al*. (2015) stated that to increase the use of TiO_2 under visible light absorption, it can take benefit of metal and non-metal dopant incorporation into TiO_2 structure. It has been found that the photocatalytic activity of TiO_2 is enhanced and effective under visible light (λ > 400 nm). Recently, TiO_2 has been doped with metal or non-metal. Several metals have been used for doping such as silver (Ag), iron (Fe), palladium (Pd), platinum (Pt),

zinc (Zn) and zirconium (Zr). Meanwhile nonmetals dopants that commonly used are boron (B), carbon (C), nitrogen (N) and fluorine (F). In addition, hybrid photocatalyst also can be used as dopant. Hybrid photocatalyst involve of incorporating semiconductors to combine the properties which in this case will give the enhancement of photocatalytic performance.

Many efforts have been done on development of TiO_2 based hybrid photocatalyst such as TiO_2-ZrO_2 (Laxmi *et al*., 2014), CuO-TiO_2, Fe_2O_3- TiO_2 and ZnO-TiO_2 (López-ayala *et al*., 2015). Several synthesis have been proposed such as TiO_2-CeF_3 by a facile one step microwave-hydrothermal synthesis (Wan *et al*., 2016), TiO_2-graphic carbon nitride (g-C_3N_4) via sol-gel method (Li *et al*., 2016), TiO_2-SiO_2, TiO_2-Al_2O_3 and TiO_2- SiO_2-Al_2O_3 prepared using a co-precipitation method (Li *et al*., 2014) . Among all the studies stated above, hydrothermal method was the favourable method due to environmental friendly, avoid problems encountered with high temperature process, able to synthesis crystal substance which are unstable near the melting point and stress-induced defects such as micro-crack that caused by phase transformation. Hydrothermal method involves of producing different chemical process flowing in aqueous solutions at temperatures above 100°C and high pressure.

This study deals a mixing of TiO_2 and its performance on the degradation of methyl orange (MO). The using of MO compare to other dyes is due to the MO is easy to get. The hybrid dopant is the mix of metal oxide and carbon. The metal oxide and carbon that will be used are alumina (Al_2O_3) and graphene respectively. Al_2O_3 is chosen due to its superb properties which are wear resistance, corrosion resistant, very stable material and robust material. Besides, Al_2O_3 is cheap compare to others and always increases in number of production every year because of various applications used in industries. Some examples of Al_2O_3 are medical implant, as coating material

and cutting tools. Graphene is used due to its properties which are good conductivity, high specific surface area and easy functionalization. Based on Baeissa (2014) graphene can lessen electron hole combination rate due to it has high electron mobility and non-metal carbon can reduce energy band gap. Graphene are used in optical electronics and also as composite material. The properties of Al_2O_3 and graphene will be an excellent photocatalyst in photocatalytic activity compare to the using of pure TiO_2 as photocatalyst. Besides, it is also can lead the TiO_2 to active under visible light irradiation.

1.2 Problem Statement

TiO_2 doped impurities is used to increase the absorbance of dyes by enhanced the activity under visible light. There are some researchers that studied the effect of TiO_2 doped Al_2O_3 (Li *et al*., 2014) and TiO_2 doped graphene (Zhang *et al*., 2011). Al_2O_3 is used due to excellent wear resistance, corrosion resistance, very stable material and robust material while graphene possess good conductivity, high specific surface and easy functionalization. Most of the researchers who involved in this primate research only study on the TiO_2 doped with other metal or non-metal but not with hybrid non-metal-non-metal. There are several methods that have been used in synthesis of doping TiO_2 such as sol gel method, hydrothermal method and co-precipitation method. Based on the studies that have been done, hydrothermal method is the best choice to synthesis the material since it have a lot of advantages such as it is safe method, eco-friendly, simple and more controllable process. Therefore, this study will focus on the effect of the presence of Al_2O_3 and graphene when mixing with TiO_2 and its absorbance of MO by hydrothermal synthesis.

1.3 Objectives

The main interest in this study is to develop the absorbance of methyl orange when TiO_2 mix with Al_2O_3 and graphene nanocomposite which is prepared by hydrothermal synthesis. Therefore, the objectives of this research are:

i. To determine the effect of hydrothermal temperature on phase identification and particle characteristics of TiO_2-Al_2O_3-graphene nanocomposite.
ii. To investigate the absorbance of methyl orange of TiO_2-Al_2O_3-graphene nanocomposite.

1.4 Expected Result

The effect of TiO_2 mix with Al_2O_3 and graphene nanocomposite by hydrothermal synthesis when conduct with temperature (200°C) and composition that were calculated according to weight percentages (wt %) using rule of mixture will be determined. From the result, the effect of mixing Al_2O_3 and graphene toward phase identification and particle characteristic will be obtained. Furthermore, the hybrid photocatalyst also will influence absorbance of TiO_2.

CHAPTER 2

LITERATURE REVIEW

2.1 Metal Oxide as Photocatalytic Materials

Metal oxide has been widely used for the photocatalytic degradation of numerous organic water contaminants and it was proved that the doped metal oxide can enhance the photocatalytic activity of the pure metal oxide (Siriwong *et al*., 2012). Recent research by Khan *et al*. (2015) reported that metal oxides have the ability to form charge carrier when stimulated with required amount energy which have been used in environmental remediation and electronic. It have been used as photocatalyst since it has light absorption properties. There are many metal oxide that normally used such as TiO_2, ZnO, SnO_2 and CeO_2. The band gap of metal oxide when use in UV light and under visible light irradiation is shown in Figure 2.1.

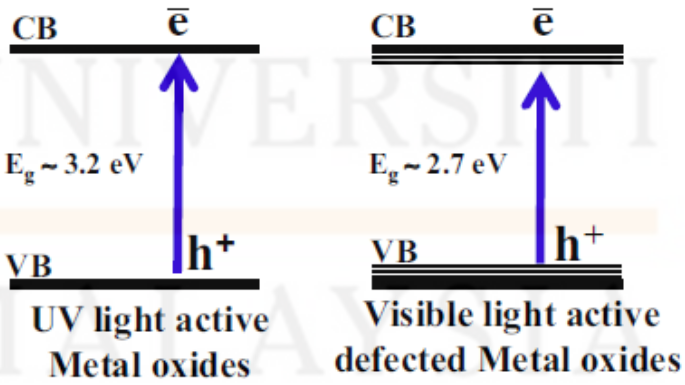

Figure 2.1: Photo excitation of metal oxides in UV light and visible light (Khan *et al*., 2015).

Wang *et al*. (2016) reported that nickel (Ni), aluminium (Al), ferum (F), gallium (Ga) and lanthanum (La) are the common metal that used as photocatalytic using hydrothermal method. It is used to tailor the band gap and electrical properties of the material which can enhance the photocatalytic activity. However, based on Shtarev *et al*. (2016) doping using different oxides such as RuO_2, V_2O_5 and Co_3O_4 can increasing the catalytic activity. This is due to the effective charge transfer between metal atoms and oxide lattice that increases the recombination time of photo excited electron-hole pairs.

In addition, mesoporous metal oxide (MMO) is gaining popularity as photocatalytic material due to its large surface area, photogenerated charge carriers transfer and carrier-induced surface reaction which give the result in photocatalytic activity (Liu *et al*., 2015). According to Cai *et al*. (2015), the combination of material zinc oxide (ZnO) with graphene become supreme as photocatalytic performance. This is because graphene can act as a charge separation in the photocatalytic process. This combination will attributed to the large surface area, excellent electron transport and lessen charge carrier recombination. Tang (2013) evaluated that ZnO is one of the semiconductor that have been successful for the using as photocatalyst.

Based on previous study by Stengl *et al*. (2013) graphene oxide (GO) has been modified as photocatalyst due to its large surface area and high activity in catalytic process. GO was prepared by safe and friendly method which can be a good support to TiO_2 in photocatalytic activity. Synthesized crystalline ZnO powder becomes good photocatalytic activity to the azodye which include the condition in visible light irradiation (Gancheva *et al*., 2016). MoO_3 nanoflake/PI that have been prepared using a facile in-situ solid-thermal give a positive result which improve of photocatalytic activity in increasing of light absorbtion (Ma *et al*., 2016).

2.2 Titanium Oxide

Titanium oxide (TiO_2), also known as titanium (IV) oxide or titania, can be found in three forms: rutile, anatase and brookite (Somani, 2006). Rutile is the most abundant of all and thermodynamically stable while anatase and brookite are unstable at all temperatures which transform to rutile when they are heated. The structure of rutile TiO_2 is shown in the Figure 2.2 and for anatase structure is shown in Figure 2.3.

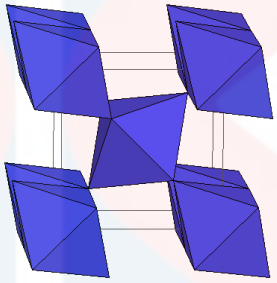

Figure 2.2: Unit cell structure of rutile TiO_2 (Somani, 2006)

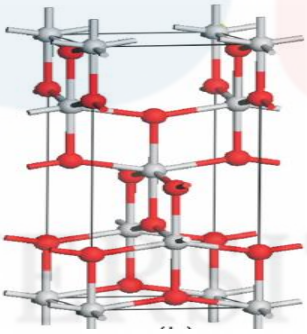

Figure 2.3: Unit cell structure of anatse TiO_2 (Yin *et al*., 2010)

TiO_2 is mostly used as photocatalyst due to its non-toxicity, low cost, chemical stability, opto-electronic properties, stability against corrosion and have excellent activity (International, 2014; Vu *et al*., 2010; Appavu *et al*., 2016). TiO_2 has a wide band gap semiconductor which rutile phase 3.00 eV, anatase phase 3.21 eV and brookite phase 3.13 eV (Shao *et al*., 2015; Appavu *et al*., 2016) which become

drawback to TiO_2 and it only active under ultraviolet (UV) light with range $\lambda < 400$ nm (Appavu *et al*., 2016).

So far, TiO_2 mostly used in wide application such as in hydrogen generation, gas sensor, and dye sensitized solar cells (Zhang *et al*., 2016). Previous research that have been studied by Haider *et al*. (2016) state that TiO_2 is the top candidate of material that have been used as a window in solar cells due to the its anti-reflection ability. This had been prove when TiO_2 doping Ni gives the result in low reflectance (25.43%) and reflective index (3.02) make a higher transmittance that make the great performance of solar cell window.

Marschall & Wang (2013) have been report about the basic principle of the photocatalysis. Using the visible light irradiation, the electron have been excited from the valence band (VB) to the conduction band (CB). It happens either the energy of the incident photon is equal or exceed the energy band gap (Eg) of the semiconductor. After the photo excitation the charge carriers can be separated and diffuse onto the particles surface, where they may perform redox catalytic reaction. The mechanism of the basic principle is shown in Figure 2.4.

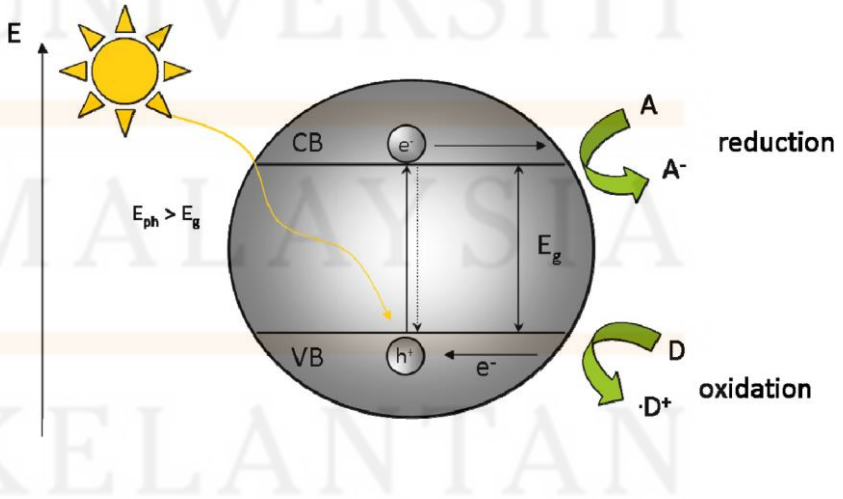

Figure 2.4: Mechanism of TiO_2 in photocatalytic activity Marshall & Wang (2013)

Figure 2.5 shows the mechanism of photocatalytic activity of nanostructured TiO_2. The visible light excites the electron from valence band and conduction band and then the electron react with water and oxygen at the surface which the redox reaction occur.

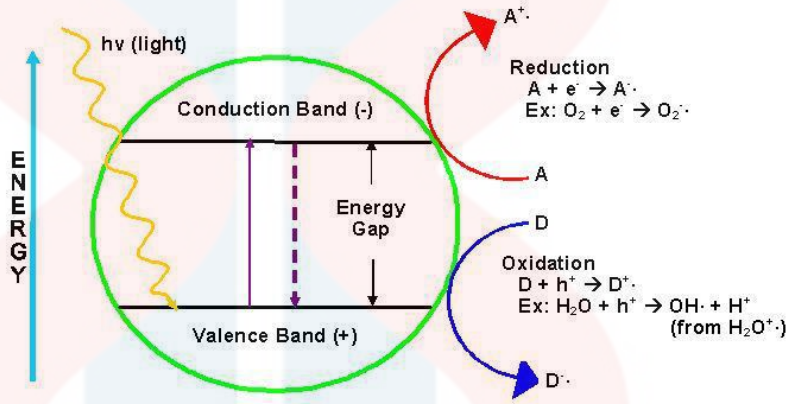

Figure 2.5: The mechanism for the photocatalytic action of nano-structured TiO_2 (Chládová *et al.*, 2011).

2.3 TiO_2 doping materials

In order to make TiO_2 active at the visible light, it must be doped with impurities either metal or non-metal. It will give the enhancement in photocatalytic activity and at the same time also will lower the band gap of TiO_2.

2.3.1 Metal Doped

Metal that usually used to doped with TiO_2 are vanadium (V), chromium (Cr), ferum (Fe), tin (Sn), silver (Ag) and zirconia (Zr). Bhange *et al.*, (2016) stated that doping 10% of Sn in TiO_2 gives the result in decreasing of band gap, increasing the surface area and the doping give the effect on transformation of anatase to rutile phase

of TiO_2. Besides, Ng *et al*. (2016) reported that Ag also gives the reduction in band gap from 3.1 eV to 2.69 eV (5 wt % Ag/ TiO_2). It drops from 3.1 eV bare TiO_2. In TiO_2 doped V, the band gap decrease from 3.26 eV to 2.85 eV which V was found to be more active compared to the bare TiO_2 (Ramacharyulu *et al*., 2014).

According to Yong *et al*. (2014) niobium (Nb) gives the reduction in band gap when dope with TiO_2. The band gap changes from 3.25 eV to 2.85 eV when anatase phase was transform into rutile phase with the increasing of Nb doping. The optical band gap energy Nb-TiO_2 was examined using UV-vis spectrophotometer. Nickel (Ni) doped TiO_2 have been great attention to be photocatalyst for degradation which improving the efficiency of photocatalyst (Yue *et al*., 2016). The schematic illustration of the photogenerated charge transfer in Ni doped TiO_2 has shown in the Figure 2.6.

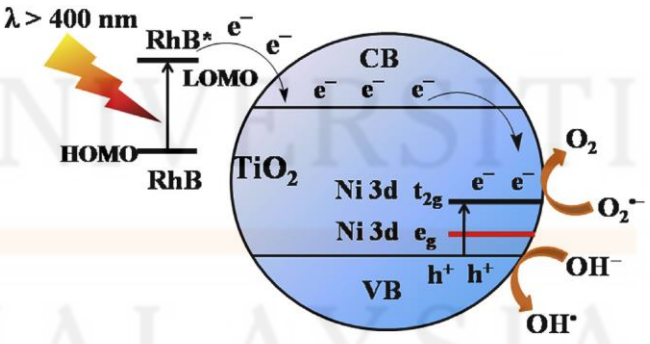

Figure 2.6: Photogenerated charge transfer events in the Ni doped TiO_2 system under visible light irradiation (Yue *et al*., 2016)

Tungsten (W) doped TiO_2 also enhanced the photocatalytic performance with the large surface area and contracted lattice which have been done by solvothermal method. The W^{6+} function as electron receiver and avoid the recombination of

electron-hole pair (Zou *et al*., 2016). Ytterbium (Yb)-doped TiO_2 were synthesized by sol-gel method exhibit a higher photocatalytic performance for methylene blue under UV irradiation (Tang *et al*., 2015).

In a study by Nitoi *et al*. (2015), doping TiO_2 with heavy metal such as Fe, Co and Ni can capably catalyze the degradation of NB under UV-Vis light irradiation. It has been introduced a new energy level (dopant impurity level) which acts as electron trap and at the same time gives enhancement of photocatalytic activity. The value of contamination is lessening compared to the un-doped TiO_2.

2.3.2 Non-metal Doped

Non-metal that commonly used to dope with on carbon (C), nitrogen (N), sulfur (S), oxygen (O) fluorine (F) boron (B) and chlorine (Cl). In a study by Chakrabortty & Gupta (2013) N doping with TiO_2 gives the reduction in band gap which is when bare TiO_2 3.17 eV and when doped with N, the band gap narrowed to 2.87 eV and 2.01 eV. Reduction of the band gap is due the excitation of an electron from valence band to conduction band in N-TiO_2 which lead to the increasing of photocatalytic activity.

Bo *et al*. (2013) evaluated that mesoporous carbon (MC) also used to support TiO_2 as photocatalyst due to its large surface area and high pore volume through a sol-gel method. The result showed that when MC doped TiO_2 it exhibits higher photocatalytic activity compared to pure TiO_2 in degradation of methyl orange. Non-metal doped are characterized by a shift from higher wavelength to the lower wavelength which cause the decrease in band gap energy (Linnik *et al*., 2015). The electron transfer of C-doped TiO_2 has shown in Figure 2.7.

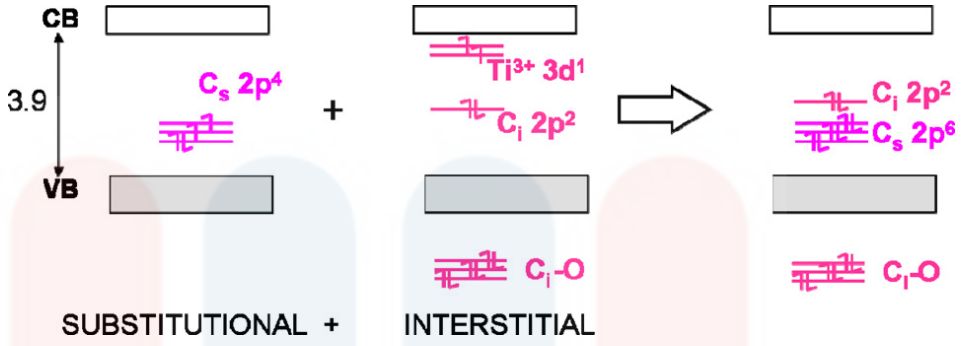

Figure 2.7: Electron transfer C-doped TiO_2 (Linnik *et al*., 2015)

2.4 TiO_2 hybrid photocatalyst

Hybrid doped or co-doped is one of the way that can modify the band gap of TiO_2 and also can accelerate the electron-hole separation. Based on previous study by Marschall & Wang (2013) co-doped which is Ni-B doped TiO_2 gives lower in band gap compared to only one dope that is B doping. When B doping TiO_2 is used, the band gap is 2.93 eV but when Ni-B doping TiO_2, the band gap reduce to 2.85 eV. Moreover, Wang *et al*. (2014) stated that C and B co-doping with TiO_2 have generate the new phase which improve photocatalytic antibacterial activity.

Mesoporous graphene and tourmaline co-doped TiO_2 give the result in reduction of band gap that is 2.28 eV which was prepared by sol-gel method (Baeissa, 2014). The study by Yang *et al*. (2013) reported that F-N co-doped TiO_2 sample give a higher photocatalytic activity when check with methylene blue under visible light irradiation. The electron transfer of N-F co-doped TiO_2 has shown in Figure 2.8.

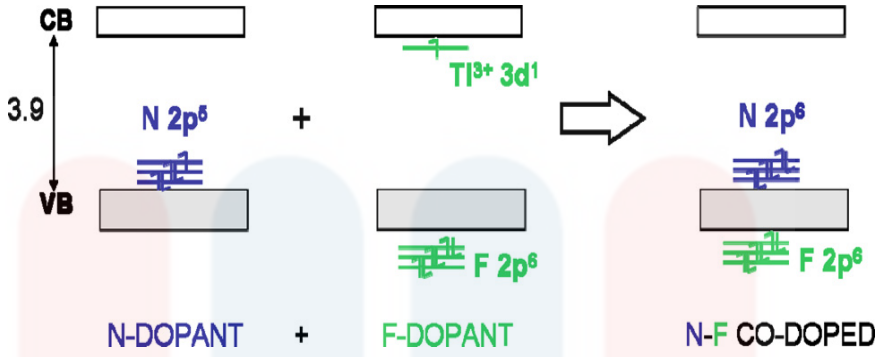

Figure 2.8: Electron transfer N-F co-doped TiO_2 (Valentin & Pacchioni, 2013)

The common tools to examine the microstructure of TiO_2 are scanning electron microscope (SEM) and transmission electron microscope (TEM). Figure 2.9 shows the microstructure of pure TiO_2 and doped TiO_2. There are different morphologies when it is compared with pure TiO_2 and doped TiO_2. Distribution of doped TiO_2 is more uniform compared to the pure TiO_2.

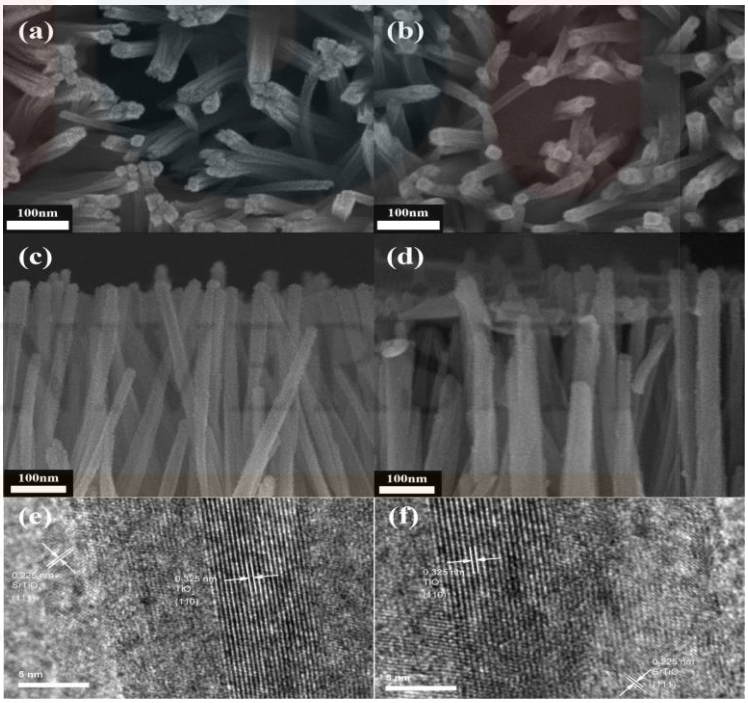

Figure 2.9: Top SEM images of (a) pure TiO_2 nanowires and (b) $SrTiO_3/TiO_2$ heterostructure. Cross-section SEM images of (c) pure TiO_2 nanowires and (d) $SrTiO_3/TiO_2$ heterostructure. (e), (f) TEM images of $SrTiO_3/TiO_2$ heterostructure (Jing *et al.* , 2015)

2.5 Synthesis Method

There are various methods that have been used for fabrication of TiO_2 hybrid photocatalyst (Momeni & Ghayeb 2016; Li *et al*., 2013; Zhang *et al*., 2015). The chosen method must has the criteria such as environmental friendly, ease of processing and cheap.

2.5.1 Hydrothermal method

Hydrothermal synthesis is the method that based on the ability of water and aqueous solutions to dilute at high temperature and pressure which the substance practically insoluble under normal conditions whereas some oxides, silicates or sulphides. The main parameters of hydrothermal synthesis are the initial pH of the medium, the duration, temperature and pressure in the system. This method is well known because the method is safe and eco-friendly.

Jeong *et al*. (2015) stated that hydrothermal method commonly used because the method is simple, high yield and more controllable process. It also offers higher surface area and low temperature sinter ability of synthesized material compared to other method. Lin & Shih (2015) reported that there are also synthesis via one-step microwave-assisted hydrothermal synthesis of nitrogen co-doped anatase TiO_2 which make the method becomes fast, simple and low cost compared other method.

In a study by Cheng *et al*. (2016) hydrothermal method produced the cerium doped TiO_2 nanopowders and it was done under alkaline conditions. Besides, it also known as simple and convenient way to prepare TiO_2 with different morphology and it provides a good circumstance for solution doping into TiO_2 nanomaterials. Moreover, based on Hu *et al*. (2016) hydrothermal method is the best method to synthesis of inorganic nanocrystal, which operate at an high temperature in a confined

volume to generate high pressure. It also can give rise to nanostructure with crystallinity without post synthetic annealing or calcination. This method is very simple, scalable and industrially compatible.

2.5.2 Sol Gel Method

Another method that commonly used to dope TiO_2 is by sol gel method. Sol gel method is a method that produces solid materials from small molecules which commonly used for fabrication of metal oxide especially for silicon and titanium. Sol-gel method is better than other which are spray pyrolysis, chemical vapor deposition and reactive magnetron sputtering. It is better due to its advantages that are simple deposition equipment, easy adjusting composition and dopants, excellent uniformity and low crystallization (Delavari *et al*., 2016).

Khalid *et al*. (2013) reported that Nd doped TiO_2 nanoparticles was synthesized using sol-gel method. Nanostructured cobalt (Co) doped ZnO thin film were deposited on glass substrate by sol gel spin coating technique. Co doped ZnO leads to band gap narrowing which enhanced the photocatalytic activity for degradation of methylene blue (MB) dye under visible light (Abdizadeh *et al*., 2011).

However, even there are a lot of advantages, there are also some lack of sol gel method. In sol gel method, the material will end up more defect at the phase composition. It may be different from desires one. Next, it needs a very high temperature furnace to get the material crystalline. Based on these disadvantages, in study of photocatalytic activity, the method that have been preferred to use is hydrothermal method compared to sol-gel method.

2.6 Degradation of dyes by TiO_2

According to Haddad *et al*. (2013) dyes are widely used in textile, paper, leather, plastic and hair colourings. There are two types of dyes which is natural and synthetic. However, synthetic dye is usually used due to its stability and low cost compared to natural dye (Yamjala *et al*., 2016). In textile industry, dye was classify based on its technique which direct dye, disperse dye and reactive dye (Semeraro *et al*., 2015). Examples of the dyes are methyl orange (MO), methylene blue (MB), congo red (CR), cibaron reactive yellow and phosphate-calcium-dye (Petcu *et al*., 2015; Lemlikchi *et al*., 2014; Appavu *et al*., 2016).

However, MO is the one of the dye that widely used in industry especially in textile industry. It has some disadvantage when using MO as a dye since it cause the dirtiness of water from the dye sewage. The chemical structure of MO is shown in Figure 2.10.

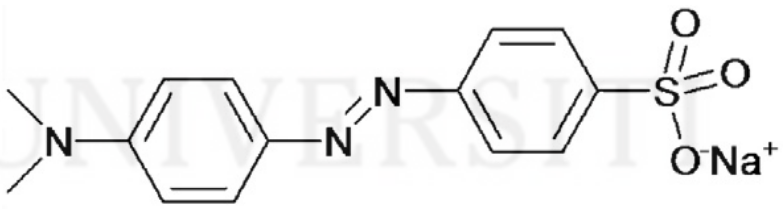

Figure 2.10: Structure of methyl orange (Filice *et al*., 2014)

2.7 Photodegradation of dye using TiO_2 hybrid nanocomposite photocatalytic

Doping TiO_2 with metal and non-metal can reduce the band gap of TiO_2 and at the same time increase the capability of photocatalytic degradation of MO. According

to Nainani *et al*. (2012) Ag doped TiO_2 enhanced the photocatalytic of MO and also lower the band gap since it can absorb wider range of UV light.

In addition, based on study by Li *et al*. (2016) g-C_3N_4/TiO_2 was used to assess the photodegradation of dye which is methylene blue (MB) that lead to enhancement of photocatalytic activity under visible light with the $\lambda > 420$ nm. It is suitable as the material for the using as photocatalyst in the photodegradation of dye in wastewater.

In addition, based on previous study by Nuengmatcha *et al*. (2016) ZnO-graphene-TiO_2 (ZGT) was used in photocatalytic degradation of rhodamine B and industrial dyes. These hybrid photocatalyst give the better result in photocatalytic degradation compared to the using of bare ZnO, graphene and TiO_2. Besides, it also suitable for the eco-friendly environmental application.

2.8 Alumina

Aluminum oxide (Al_2O_3) also known as alumina made by the metal aluminum which happens in nature as the mineral corundum (Al_2O_3); diaspora ($Al_2O_3.H_2O$); gibbsite ($Al_2O_3.3H_2O$) and most commonly as bauxite, which is an impure form of gibbsite (Davis, 2010). There are two types of Al_2O_3's structure, hexagonal and octahedral that become holder of the atom.

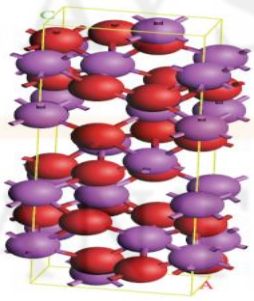

Figure 2.11: The unit cell structure of Al_2O_3 (Yan & Wei, 2014)

Al_2O_3 is very hard material and the hardness is only exceed by diamond. Besides, it have a great properties which there are high mechanical strength, corrosion resistance, bio inertness, wear resistance, high Young modulus and stiffness (Somani, 2006). These properties make Al_2O_3 has been used in wide application. Mostly it is used in biomedical implant such as dental implant and prosthetic implant. It is suitable due to its biocompatibility and not harmful to human body.

Besides, Al_2O_3 also used as a dopant. In a study by Su *et al*. (2015) Al_2O_3 is doped with α-Fe_2O_3 in order to increase the properties of ethanol sensing. The doping of Al_2O_3 make α-Fe_2O_3 better sensitive to ethanol that make it suitable to use for ethanol sensor. In addition, Al_2O_3 also used as dopant material for enhancement of photocatalytic activity of tungsten. This was reported by Stojadinović *et al*. (2016) which is when tungsten doped Al_2O_3/ZnO the photocatalytic activity is higher compared to undope Al_2O_3/ZnO.

2.9 Graphene

Graphene is a thin layer of pure single atom carbon, tightly packed layer of carbon atoms which attached together in a hexagonal honeycomb lattice. Previous study by Liao & Duan (2012) stated that graphene is a unique material that is form a single atomic sheet of sp^2 bonded carbon. The illustration of graphene is shown in Figure 2.12.

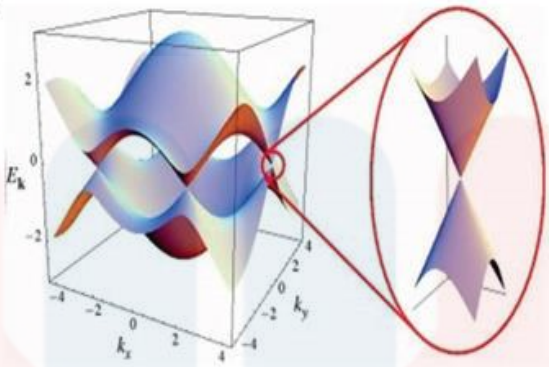

Figure 2.12: Illustration of graphene as single atomic sheet of sp^2 bonded carbon (Liao & Duan (2012)

Besides, it also have an excellent properties which are superb mechanical strength, electrical and thermal conductivity, optical transparency, chemical stability and impermeability. Due to these properties, graphene had been used in various application, for examples are nanofiller of composites, ultra high frequency transistors, gas sensor and potential electrode material (Zhang *et al*., 2015).

Moreover, graphene also can be used as a dopant as catalyst in order to increase the photocatalytic degradation of dye. Based on Nuengmatcha *et al*. (2016) ZnO-graphene-TiO_2 (ZGT) had been efficiently synthesized via solvothermal method. Graphene has been used as dopant in ZnO and TiO_2 to enhance the photocatalytic performance due to the drawback that have in the ZnO and TiO_2. Graphene showed a great performance in photodegradation since it can scavenge and shuttle electron simultaneously which lead to minimize the recombination issues.

CHAPTER 3

MATERIALS AND METHODOLOGY

3.1 Introduction

This chapter explains about the materials and method that has been used in this study. Overall of this experimental work was conducted in the laboratory of Universiti Malaysia Kelantan, Jeli Campus. The experiment was conducted in three stages which were preparation, characterization and photocatalytic study. The overall experiment in in this study was shown in Figure 3.1.

3.2 Raw Materials

TiO_2 (99.5% purity, average particle size >21 nm), Al_2O_3 (99.9% purity, average particle size >20 µm) and graphene nanoplates (99.9% purity, average particle size > 10 nm) had been used for preparation of nanocomposite and was purchased from Sigma Aldrich.

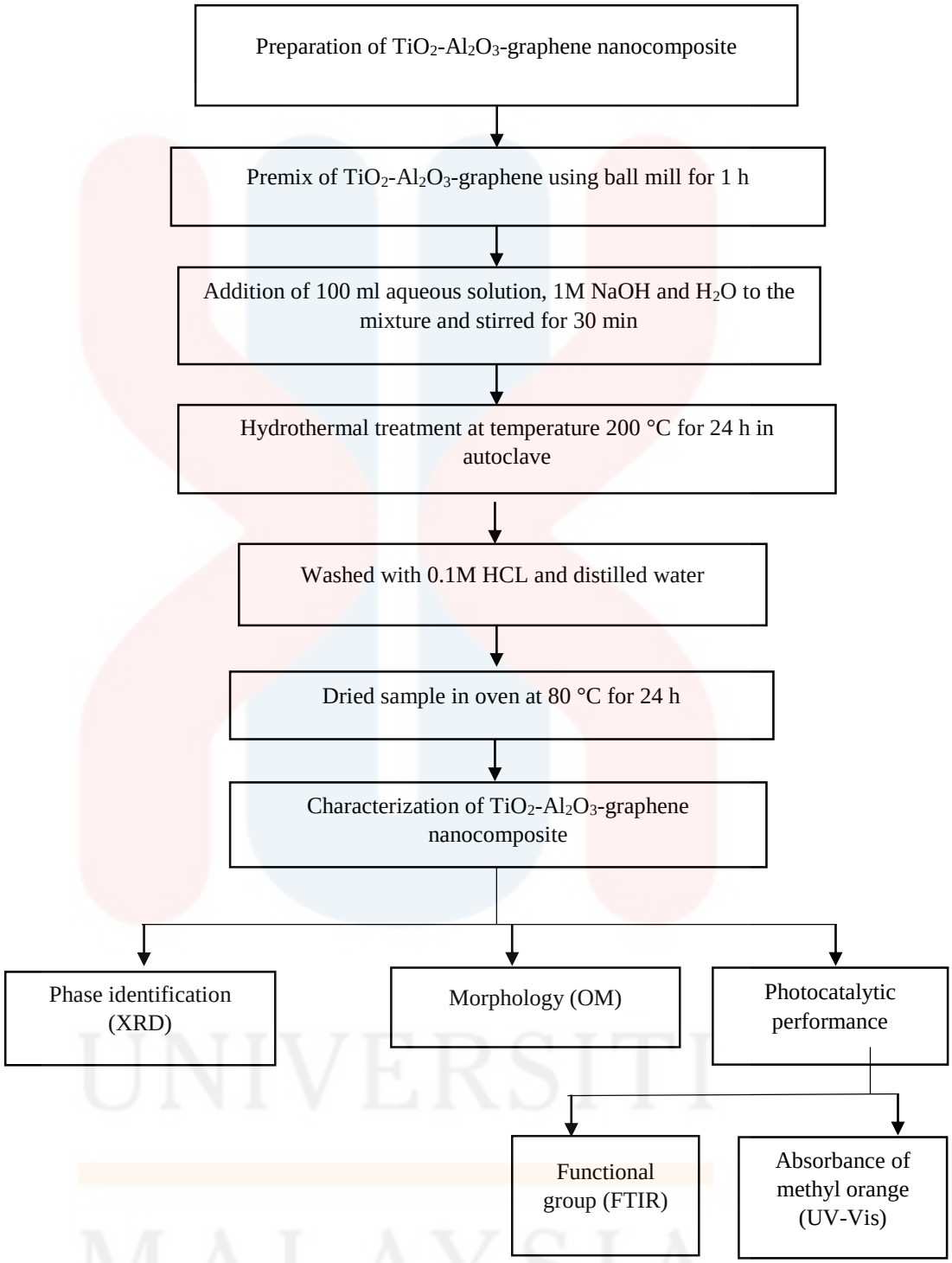

Figure 3.1: Research flow chart

3.3 Preparation of TiO_2-Al_2O_3-Graphene Mixture

TiO_2, Al_2O_3 and graphene powder mixture were calculated according to weight percentage (wt %) used rule of mixture as shown in Table 3.1. The preparation of the composition had been divided into six samples which the two samples as controlled experiment. The controlled experiment in this study were 100% TiO_2 and TiO_2-Al_2O_3 with (60-40).

Table 3.1: The composition of TiO_2-Al_2O_3-graphene

Material / Sample	TiO_2 (wt %)	Al_2O_3 (wt %)	Graphene (wt %)
P100	100	0	0
TA60	60	40	0
TAG80	80	15	5
TAG70	70	20	10
TAG60	60	30	10
TAG50	50	30	20

Each set of compositions had been premixed using ball mill for 1 h to obtain homogenous particle distribution.

3.4 Hydrothermal Method

The composition of TiO_2, Al_2O_3 and graphene powders had mixed with 1 M NaOH. The mixture was stirred for 30 minutes and subjected to hydrothermal treatment at temperature 200 °C for 24 h in an autoclave. After the reaction complete, the sample was collected and washed using 0.1 M HCL (200 ml). This followed by washed with distilled water until a pH 7 of washing solution was obtained. The final product was obtained and dried in the oven at 80°C for 24 h.

3.5 Characterization

3.5.1 Phase identification

The X-ray diffraction (XRD) was used for determination of phase identification of synthesized TiO_2-Al_2O_3-graphene nanocomposite. This was perform using Bruker D2 Phaser with Cu Kα radiation (ƛ = 0.154 nm) with the step size is 0.02° and the range of 2θ angle was between 10° to 90°. Any peaks that has been present was estimated as correct match of the peak position. DIFFRAC.EVA software was used which show the peak intensity that refer to crystal structure and qualitative analysis.

3.5.2 Crystallite size and Internal Strain

Williamson-Hall (WH) method was used to calculate the crystallite size and internal strain of the nanocomposites. The value of crystallite size depends on the size of the peak which the broader the peak, the smaller the crystallite size. The formula of the WH method was shown in equation 1 (Saranya *et al*., 2014):

$$B_r \cos\theta = \left(\frac{k\lambda}{D}\right) + \eta \sin\theta \qquad \text{Eq. 1}$$

where B_r = overall broadening

k = 0.9 is a shape factor for spherical particles

ƛ = is the wavelength of the incident radiation (ƛ = 0.154nm)

D = intercept of the graph

n = internal strain

Ø= is half of the position 2 theta angle

The full width at half maximum (FWHM) and Obs. Max value was determined from DIFFRACT.EVA software. Then, according to Eq. 1, $B_r \cos\theta$ against $\sin\theta$ was plot. The slope was given the internal strain whereas intercept was used to calculate crystallite size. All of the composition were calculated according to hkl $(10\bar{1})$ and (200).

3.5.3 Morphology (OM)

To evaluate the particle size of composition, the images was observed under optical microscope (OM) of metallurgical microscope model MT8100 was used. The OM was for transmitted illuminator with 100-240V 50/60Hz 6V 30W. Magnification that has been used for observed was 20X. Jenoptik progress software was used when observed the morphology of particle size.

3.6 Functional Group

In addition, Fourier transform infrared (FTIR) spectrometer was used to determine the adsorption of organic molecules in raw materials and nanocomposite. FTIR spectra was evaluated using Thermo Scientific^{TM} iD7 with single-bounce attenuated total reflectance (ATR) technique. The FTIR spectra were recorded in the scanning range of 400-4,000 cm^{-1} at 4 cm^{-1} with 16 scans. The analysis of infrared spectra on the raw materials and nanocomposite were done using OMNIC spectra software.

3.7 Absorbance of Methyl Orange

The performance of TiO_2-Al_2O_3-graphene nanocomposite in visible light was studied using methyl orange (MO) dye. 20 ppm MO dye solution was prepared using 100 ml distilled water and 0.2 mg of MO. Then, 0.1 g nanocomposite was added to the dye solution. The suspension was subjected to visible light irradiation for 60, 120 and 180 minutes. Throughout the experiment, the aqueous suspension was magnetically stirred. The percentage of MO absorbance was calculated using the formula in Eq. 2:

$$\text{Photocatalytic absorbance (\%)} = \left(\frac{Co - C}{Co}\right) \qquad \text{Eq.2}$$

where C_o is the initial absorbance of MO and C is the absorbance of MO after "t" minute's irradiation. The absorbance was measured using UV-VIS Spectrometer (HACH DR 5000). In the case of this composition, the absorption edge appeared in UV-Vis region (wavelength of 457nm).

CHAPTER 4

RESULTS AND DISCUSSION

4.1. Introduction

This chapter discusses the results obtained from the experimental work from Chapter 3 for absorbance of methyl orange using TiO_2-Al_2O_3-graphene nanocomposite prepared by hydrothermal synthesis. First part describes the phase identification and followed by crystallite size and internal strain of raw materials and nanocomposite powder after hydrothermal. Second part presents morphology of the powder using optical microscope. Next, the functional group determination using FTIR analysis and absorbance of methyl orange of nanocomposite using UV-VIS.

4.2. Phase Identification

Figure 4.1 shows the X-ray diffraction patterns of raw TiO_2, Al_2O_3 and graphene powders. The XRD pattern of raw powder was used as a reference sample in order to compare the nature of broadening. In XRD patterns of TiO_2 powder, three major peaks could be resolved at 25.3°, 47.945° and 62.637°. All peaks were assigned to anatase TiO_2 and no peaks of brookite or rutile TiO_2 was visible in the pattern. The crystal system for TiO_2 was tetragonal. Peaks identified as corundum Al_2O_3 shows the peaks at 2θ about 24.435°, 35.043°, 37.694°, 43.260°, 52.537° and 57.506° in hexagonal structure. In graphene patterns, there were only one peak visible (26.133°) with hexagonal structure.

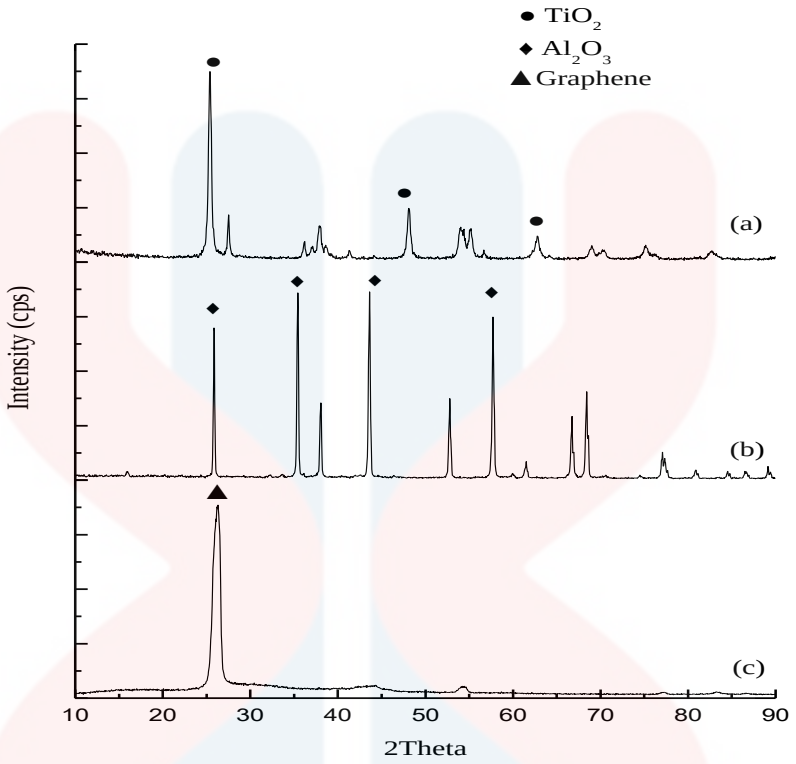

Figure 4.1: X-ray diffraction pattern of raw powder (a) TiO_2, (b) Al_2O_3 and (c) graphene

XRD pattern of nanocomposite with different composition is shown in Figure 4.2. In Figure 4.2 (a), two peaks of anatase TiO_2 was found at 25.3° and 48.020° with small shift to the right indicating the changes in TiO_2 structure when doping with Al_2O_3. However, the intensities of the peaks of TiO_2 doping Al_2O_3 was low compared to that of raw TiO_2 and Al_2O_3 powders. This could be explained by contribution of Al_2O_3 doping to the broadening of XRD pattern. Broadening of the peaks increased indicating that the crystallinity of the nanocomposites decreased with the Al_2O_3 addition.

In Figure 4.2 (b), the peaks of TiO_2 was different with the peaks of TA60. For TiO_2, the number of peaks were shown same with TA60 and the peaks were at 2θ = 25.3° and 48.028° with d = 3.51741 and 1.8928° Å. In addition, the peaks assigned at 2θ = 25.527°, 35.07°, 43.386° and 57.526° was identified as Al_2O_3. The peaks for

graphene were at 2θ = 26.512° and 43.448° with d = 3.35933 and 2.08113 Å. There was a different with raw graphene in Figure 4.1 which the peaks of raw graphene shown only at one peaks, but in TAG80 the peaks of graphene shown in two peaks which $(\bar{1}\bar{1}\bar{1})$ and $(\bar{1}00)$. The peaks of TAG80 has as little to the right compared to the peaks of TA60.

Figure 4.2 (c) referred to the composition of TAG70. The peaks that clearly shown was less compared to the peaks that shown in TA60 and TAG80. XRD patterns for TiO_2 was assigned at 2θ = 25.666° and 38.393° with d = 3.46813 and 2.34272 Å. The value of 2θ for TiO_2 increased compared to the pure TiO_2, TA60 and TAG80. Another different that can be detected in TAG70 was for Al_2O_3, there were only two peaks could be resolved which were at 2θ = 25.765° and 48.557° with d = 3.45503 and 1.87341 Å. The peaks of graphene in TAG70 increased 0.11° compared in pure graphene. The crystal structure for TiO_2, Al_2O_3 and graphene were remained after hydrothermal process.

In Figured 4.2 (d), the peaks of TiO_2 clearly was sharp compare to TAG70 which TAG70 peaks which had two peaks but for TAG60 there were three peaks at $(10\bar{1})$, (200) and $(\bar{2}04)$. The number of peaks was similar with raw TiO_2 in Figure 4.1 and there was a little shift to the right on peak position. In Al_2O_3 XRD patterns, peaks at 2θ = 35.204°, 43.431° and 57.681° with d = 2.54725, 2.08097 and 1.59882 Å were observed. The peaks of Al_2O_3 only shown clearly at three peaks compared to the peaks at pure Al_2O_3, TAG80 and TAG70 which consists of four peaks. In addition, for graphene there were two peaks which at 2θ = 26.595° and 43.452 with d = 3.34898 and 2.08097 Å. But, the intensity of 2θ = 26.595° was higher than 2θ = 43.452°.

For Figure 4.2 (e) the composition assigned for TAG50. All the peaks for TiO_2, Al_2O_3 and graphene shows less compared to the Figure 4.1, TAG80, TAG70 and TAG60. There were only one peaks for TiO_2 which at $2\theta = 25.283°$ with d = 3.51977 Å can be detected. The peaks for Al_2O_3 and graphene both XRD patterns that clearly shown were two. For Al_2O_3 the peaks were at $2\theta = 43.432°$ and 57.608° with d = 2.08185 and 1.59875 Å. The value of 2θ had only a bit different compared to the value 2θ of TAG60. While for graphene, the peaks were at $2\theta = 26.590°$ and 43.454° with d = 3.34965 and 2.08086 Å. It was vice versa to the Al_2O_3 because the peaks at 2θ of graphene was decreased and for Al_2O_3 was increased. The crystal structure for TiO_2, Al_2O_3 and graphene were also not changed.

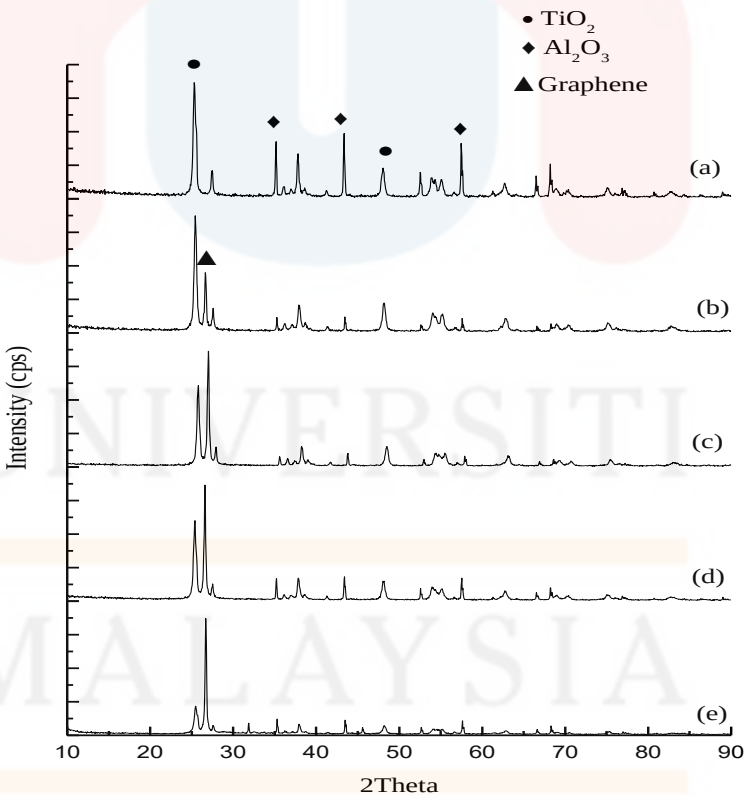

Figure 4.2: XRD pattern of composition (a) TA60, (b) TAG80, (c) TAG70, (d) TAG60 and (e) TAG50

4.3. Crystallite Size of Nanocomposite

Crystallite size of TiO_2 is shown in Figure 4.3. It was calculated using Williamson-Hall (WH) method. The data derived from WH method were plotted $B_r \cos\theta$ against $\sin\theta$. It was observed the plot is linear indicating that structure refinement was not only originated from crystallite size but also the internal strain. Table 4.1 shows the crystallite size and internal strain of TiO_2. Nanocomposite composed of only Al_2O_3 has lower crystallite size compared to that of the other nanocomposites as a result of higher composition of Al_2O_3. The intensity of the Al_2O_3 decreased shows the presence of Al^{3+} by the octahedral and tetrahedral sites (Deraz & Alarifi 2012). In terms of different compositions of TiO_2 in nanocomposite, decreasing TiO_2 content exhibited lower crystallite size. At higher TiO_2 content, TiO_2 tend to form larger crystallites (Geantet *et al*., 1995).

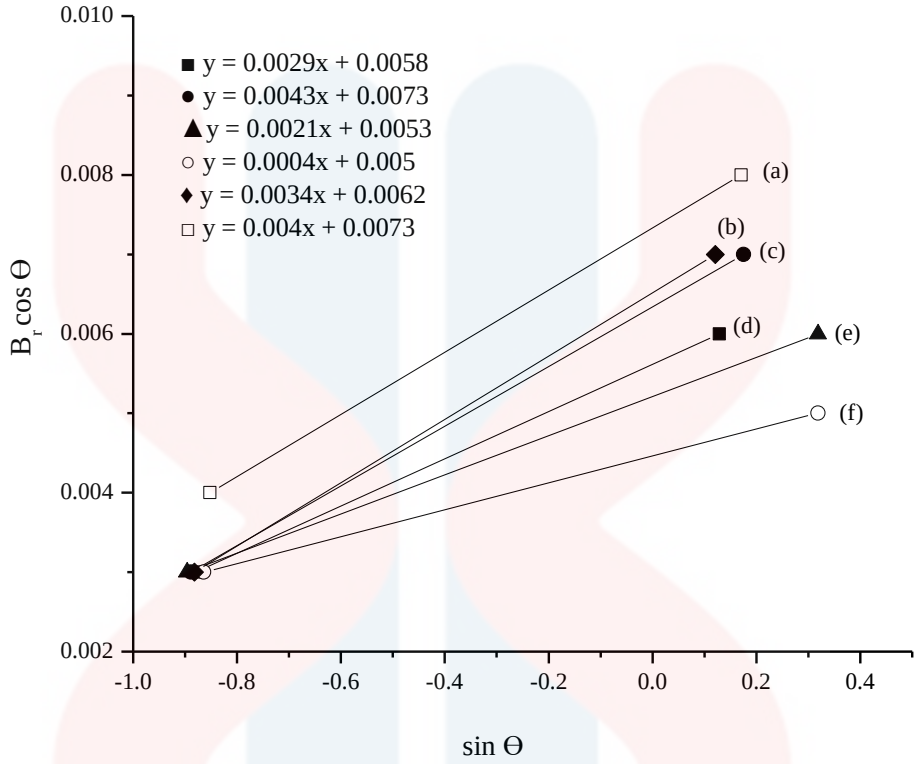

Figure 4.3: Plot of $B_r \cos\theta$ against $\sin\theta$ of different nanocomposite (a) TAG50, (b) TAG60, (c) TA60, (d) T100, (e) TAG80 and (f) TAG70

Table 4.1: Crystallite size of nanocomposites

Composition	Crystallite size (nm)	Internal Strain
T100	22.94	0.0029
TA60	18.38	0.0043
TAG80	25.39	0.0021
TAG70	26.64	0.0004
TAG60	21.78	0.0034
TAG50	18.28	0.004

4.4. Morphology of Nanocomposites

Morphology of raw TiO_2, Al_2O_3 and graphene powders were captured under optical microscope as shown in Figure 4.4. Different particle size and shape were resolved under magnification 20X. The microstructure consists of particles size of TiO_2, Al_2O_3 and also graphene. TiO_2 has smallest particle size followed by Al_2O_3 and then the largest particle size was graphene. The particle size of the graphene was the largest due to agglomeration since graphene among of the lightest materials and tend to agglomerate.

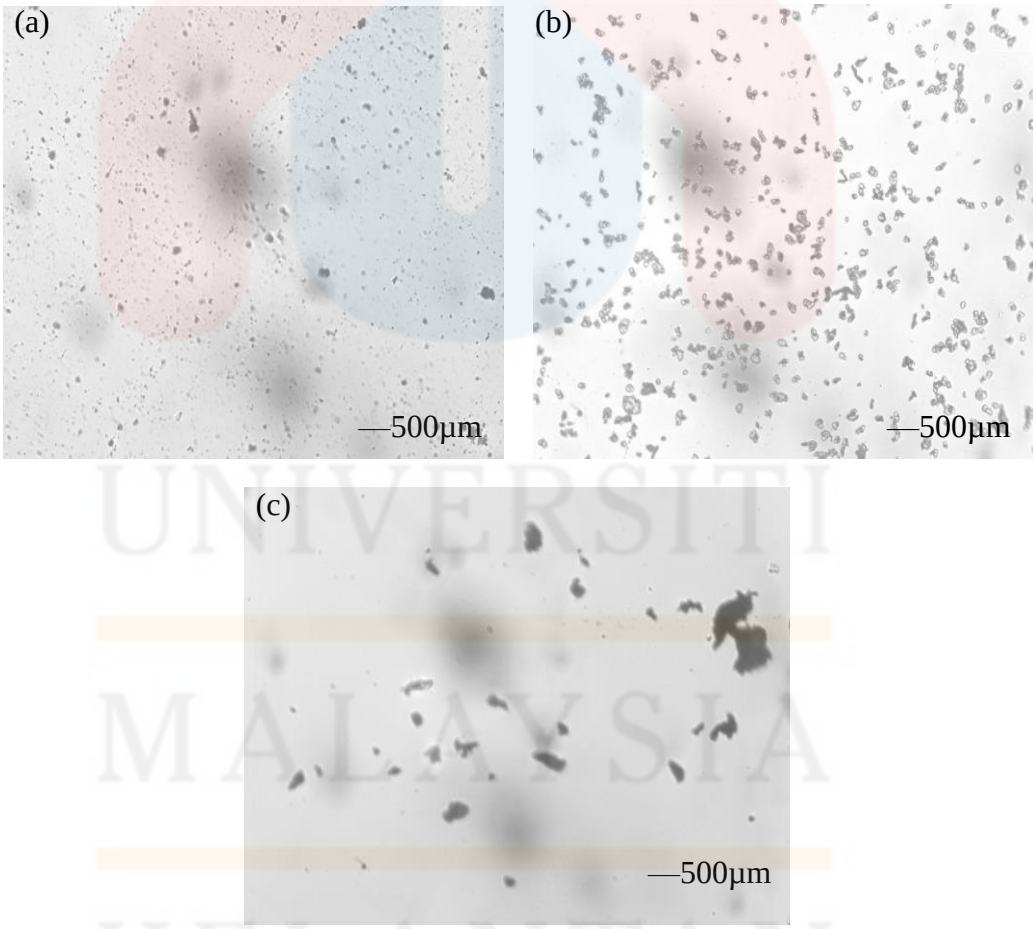

Figure 4.4: Optical microscope images of (a) TiO_2, (b) Al_2O_3 and (c) graphene

Figure 4.5 shows the morphology images of different nanocomposite composition prepared. Particle size of raw TiO_2, Al_2O_3 and graphene clearly can be detected since all of the nanocomposites have different particle size (Figure 4.4). However, in Figure 4.5 (a), the nanocomposite consists of only TiO_2 and Al_2O_3 had the lowest particle size than that of the other nanocomposites. In the images of TiO_2 doped Al_2O_3 and graphene nanocomposite, the particle size was quite similar and graphene obviously can be seen since it has the largest particle size compared to TiO_2 and Al_2O_3 particles.

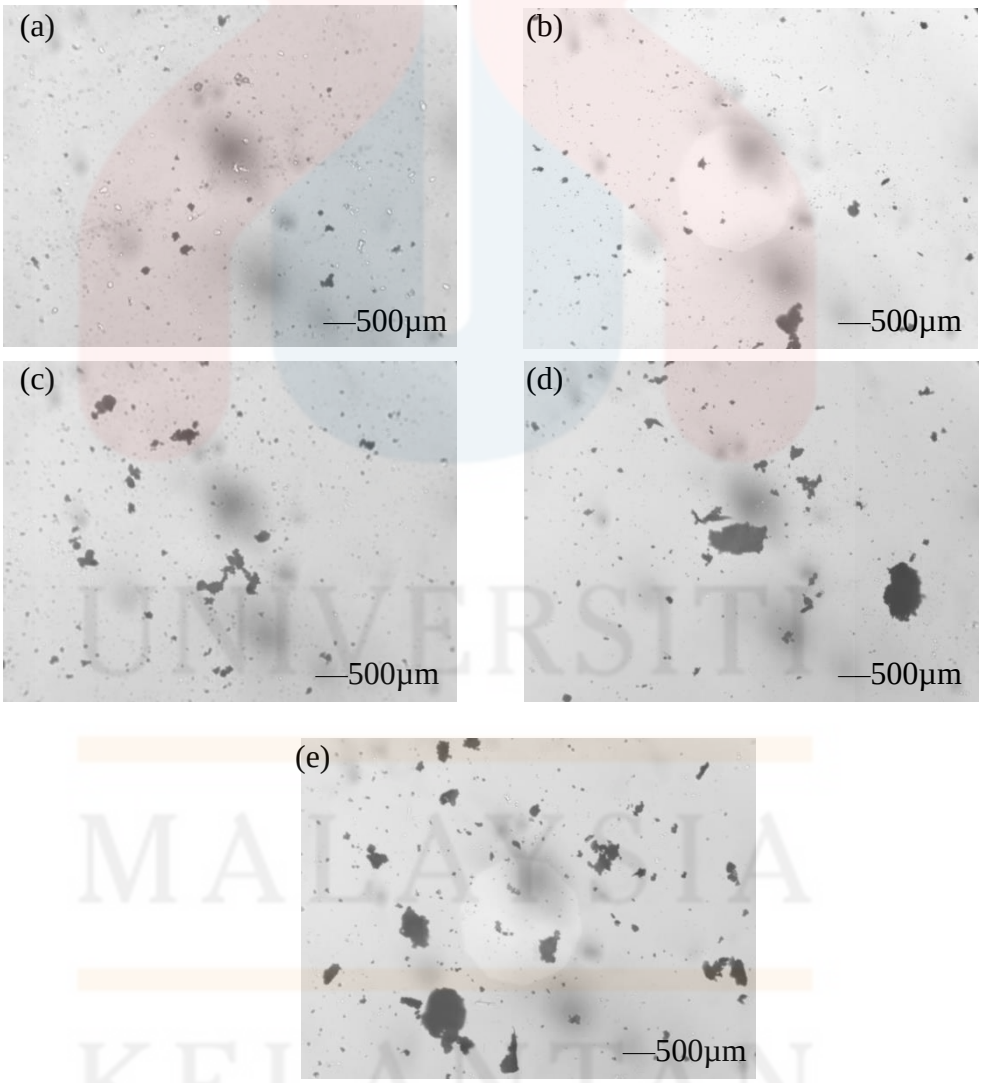

Figure 4.5: Optical microscope images of nanacomposite (a) TA60, (b) TAG80, (c) TAG70, (d) TAG60, (e) TAG50

4.5. Functional Group of TiO_2-Al_2O_3-Graphene Nanocomposites

The infrared spectrum for raw TiO_2, Al_2O_3 and graphene powders is shown in Figure 4.6. The infrared spectra of anatase TiO_2 showed a broad band between 3000 cm^{-1} and 3600 cm^{-1}. The spectra attribute O-H group at wavenumber of 3365.79 cm^{-1} which due to the absorption of water molecule during washed (Roy, 2013). Presence of hydroxyl group produced wide broadening of the peak. In addition, the N-H group was detected at wavenumber 1638.43 cm^{-1}. The N-H stretching mode in TiO_2 was referred to the aliphatic primary amides which happen due to the reaction of powder with acid. Besides, the N-H group shown at a shallow peak which between 1500 cm^{-1} and 1580 cm^{-1} which vice versa from the broadening peak of O-H group. For raw Al_2O_3, there were not bonding detected since the peaks was flat. In graphene spectral, the functional group of inorganic nitrate was detected at wavenumber of 1684.92 cm^{-1}.

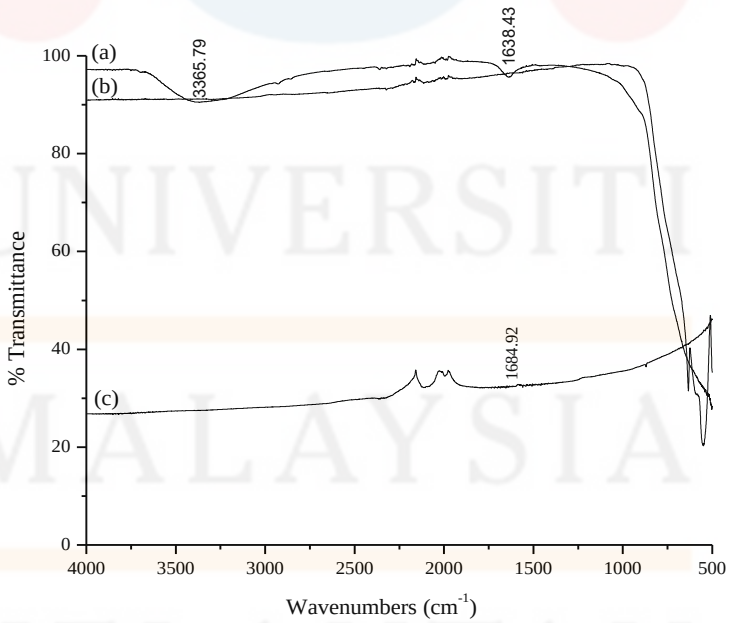

Figure 4.6: FT-IR spectral for raw (a) TiO_2, (b) Al_2O_3 and (c) graphene

Figure 4.7 showed the infrared spectra of different compositions of the nanocomposites. The functional group that presence in all compositions were almost similar which were primary aliphatic alcohol (O-H) and aliphatic primary amide (N-H). In Figure 4.7 (a), the O-H group was presence at the wavenumber of 3353.54 cm^{-1}. The N-H group detected at wavenumber 1632.10 cm^{-1}. While in TAG80, O-H groups was presence at wavenumber of 3342.41 cm^{-1}, N-H group and terminal venyl olefins detected at wavenumbers 1631.37 cm^{-1}. In addition, for TAG70 the peaks at 3339.23 cm^{-1} and 1634.75 cm^{-1} which indicates the presence of O-H group and N-H group.

The functional group for TAG60 detected was only N-H group at wavenumber of 3349.77 and 1633.85 cm^{-1} meanwhile for TAG50, the N-H group were presence at the wavenumbers of 3175.88 and 1632.45 cm^{-1}. Besides, the inorganic carbonate also detected at 1374.49 cm^{-1}. Compare to the other compositions, TAG50 was the only composite consist of inorganic carbonate due to the carbon hydrogen stretching (Coates *et al.*, 2000). All of the bonding presence was affected by the hydration state of the composition.

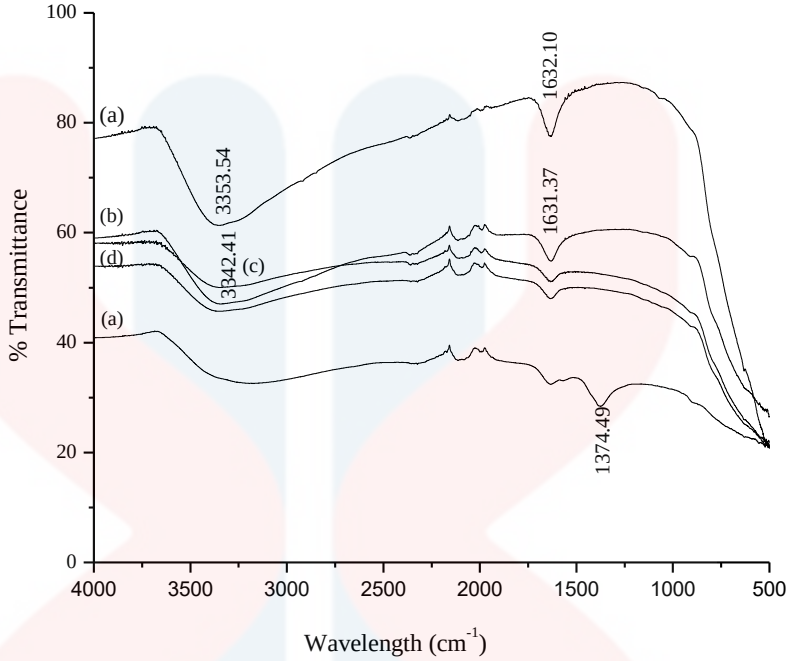

Figure 4.7: FTIR spectral for (a) TA60, (b) TAG80, (c) TAG70, (d) TAG60 and (e) TAG50

4.6. Absorption of Methyl Orange using TiO_2-Al_2O_3-Graphene Nanocomposite

UV-Vis absorption spectra of different nanocomposite compositions is shown in Figure 4.8. The degradation of methyl orange was left for 3 hours. The methyl orange showed a maximum absorption at 457 nm and at 3 hour. The absorbance of the MO did not change when there are no catalyst is presence. The addition of Al_2O_3 and graphene in nanocomposite change the percentage of MO absorbance. TA60 nanocomposite gave greater absorbance than nanocomposite (32.384%) in visible light region. This was followed by TAG50 nanocomposite (29.89%). In addition, mixing of graphene with TiO_2 decreased the absorption percentage in visible light region. However, when TiO_2 mix with Al_2O_3 and graphene the percent of absorption TAG50 shows the best absorption compared to the other nanocomposite which mean that the

increased in the amount of graphene lead the best absorption. The least amount of graphene used which gave the least percent of absorption is TAG80 that is only 1.002%.

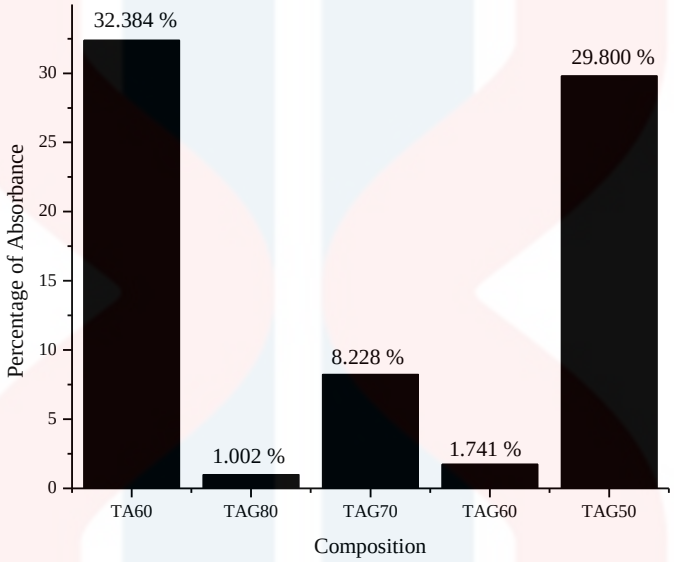

Figure 4.8: Absorbance percentage of methyl orange with different composition for 3 h

CHAPTER 5

CONCLUSION

5.1 Conclusion

In this study, the absorbance of the TiO_2-Al_2O_3-graphene nanocomposite by hydrothermal synthesis have been successful investigated. Different composition of the nanocomposite have been conducted The conclusions were drawn from the morphology, phase indentification, crystallite size, functional group and absorbance of MO of different composition of the nanocomposite, states as follow:.

1. No new phase was formed in TiO_2-Al_2O_3-graphene nanocomposite using 200°C of hydrothermal.
2. All nanocomposite were confirmed as nanostructured materials but, nanocomposite with composition of 70 wt% TiO_2, 20 wt% Al_2O_3 and 10 wt% graphene (TAG70) showed the lowest crystallite size (26.64 nm).
3. The presence of O-H, N-H, and inorganic carbonate in the nanocomposite after hydrothermal synthesis was obtained.
4. The highest absorbance was achieved by 60 wt% of TiO_2 of composite with only 40 wt% Al_2O_3 (32.813%).

5.2 Suggestion for Future Works

This work was carried out only the absorbance of the photodegradation of MO under visible light, so further it should be studied on photocatalytic degradation of dyes using UV region. The result only showed the effect of TiO_2-Al_2O_3-graphene

when exposed to the visible light. The absorbance of MO might be increased when using UV-Vis lamp and this is also will increase the photocatalytic activity. Moreover, only one parameter which is different composition that have been used in this study, so several some parameter should be include in the further research such as different temperature and irradiation light intensity. Besides, the using of OM in determine the particle size of nanocomposite might be replace by SEM since SEM have a better quality of image compared to OM.

REFERENCES

Abdizadeh, H., Ashuri, M., Tavakoli, P., Nouribahadory, A., & Reza, H. (2011). Improvement in physical and mechanical properties of aluminum/zirconia composites fabricated by powder metallurgy method. *Materials and Design*, *32*(8–9), 4417–4423.

Appavu, B., Kannan, K., & Thiripuranthagan, S. (2016). Enhanced visible light photocatalytic activities of template free mesoporous nitrogen doped reduced graphene oxide/titania composite catalysts. *Journal of Industrial and Engineering Chemistry*, 1–8.

Baeissa, E. S. (2014). Green synthesis of methanol by photocatalytic reduction of CO_2 under visible light using a graphene and tourmaline co-doped titania nanocomposites. *Ceramics International*, *40*(8 Part A), 12431–12438.

Bhange, P. D., Awate, S. V, Gholap, R. S., Gokavi, G. S., & Bhange, D. S. (2016). Photocatalytic degradation of methylene blue on Sn-doped titania nanoparticles synthesized by solution combustion route. *Materials Research Bulletin*, *76*, 264–272.

Bo, Y. I. N., Ji-tong, W., Wei, X. U., Dong-hui, L., & Wen-ming, Q. (2013). Preparation of TiO_2/mesoporous carbon composites and their photocatalytic performance for methyl orange degradation. *New Carbon Materials*, *28*(1), 47–54.

Cai, R., Wu, J., Sun, L., Liu, Y., Fang, T., Zhu, S. & Wei, A. (2015). 3D graphene/ZnO composite with enhanced photocatalytic activity. Nu Sc. *Jmade*, 2–4.

Chakrabortty, D., & Gupta, S. Sen. (2013). Photo-catalytic decolourisation of toxic dye with N-doped titania : A case study with Acid Blue 25. *Journal of Environmental Sciences*, *25*(5), 1034–1043.

Chen, C., Liu, J., Liu, P., & Yu, B. (2011). Investigation of Photocatalytic Degradation of Methyl Orange by Using Nano-Sized ZnO Catalysts. *Advanced in Chemical Engineering and Science*, *2011*(January), 9–14.

Cheng, Y., Zhang, M., Yao, G., Yang, L., Tao, J., Gong, Z., & He, G. (2016). Band gap manipulation of cerium doping TiO_2 nanopowders by hydrothermal method. *Journal of Alloys and Compounds*, *662*, 179–184.

Chládová, A., Wiener, J., & Poláková, M. (2011). Testing the photocatalytic activity of TiO_2 nanoparticles with potassium permanganate solution. *Brno, Czech Republic,Eu*. *9*, 2–6.

Davis, K. (2010). Material Review : Alumina (Al_2O_3), 109–114.

Delavari, S., Aishah, N., Amin, S., & Ghaedi, M. (2016). Photocatalytic conversion and kinetic study of CO_2 and CH_4 over nitrogen-doped titania nanotube arrays. *Journal of Cleaner Production*, *111*, 143–154.

Deraz, N. M., & Alarifi, A. (2012). Processing and evaluation of alumina doped nickel ferrite nano-particles. *International Journal of Electrochemical Science*, *7*(5), 4585–4595.

El Haddad, M., Slimani, R., Mamouni, R., ElAntri, S., & Lazar, S. (2013). Removal of two textile dyes from aqueous solutions onto calcined bones. *Journal of the Association of Arab Universities for Basic and Applied Sciences*, *14*(1), 51–59.

Filice, S., Angelo, D. D., Libertino, S., Nicotera, I., Kosma, V., Privitera, V., & Scalese, S. (2014). Graphene oxide and titania hybrid Nafion membranes for efficient removal of methyl orange dye from water. *Carbon*, 7–8.

Gancheva, M., Atanasova, G., Kovacheva, D., Uzunov, I., & Cukeva, R. (2016). Design and photocatalytic activity of nanosized zinc oxides. *Applied Surface Science*, 5–22.

Geantet, C., Afanasiev, P., Breysse, M., & des Courières, T. (1995). Soft chemistry route for the preparation of highly dispersed transition metals on zirconia. *Studies in Surface Science and Catalysis*, *91*(C), 273–280.

Haider, A. J., Najim, A. A., & Muhi, M. A. H. (2016). TiO_2/Ni composite as antire fl ection coating for solar cell application. *Optics Communications*, *370*, 263–266.

Hu, C., Lu, T., Chen, F., & Zhang, R. (2016). A brief review of graphene – metal oxide composites synthesis and applications in photocatalysis. *Journal of the Chinese Advanced Materials Society* 33(1), 20–39.

International, A. (2014). Effect of Preparation Method on Optical and Structural Properties of TiO_2/ZrO_2. *Nanocomposite*, *33*(1), 27–33.

Jeong, Y., Balamurugan, C., & Lee, D. (2015). Enhanced CO_2 gas-sensing performance of ZnO nanopowder by La loaded during simple hydrothermal method. *Sensors & Actuators: B. Chemical*, 2–3.

Jing, F., Zhang, D., Li, F., Zhou, J., & Sun, D. (2015). High performance ultraviolet detector based on $SrTiO_3$/TiO_2 heterostructure fabricated by two steps in situ hydrothermal method. *Journal of Alloys and Compounds*, *650*, 97–101.

Jr, N. C., Perera, S., & Gillan, E. G. (2015). Journal of Solid State Chemistry Rapid solid-state metathesis route to transition-metal doped titanias. *Journal of Solid State Chemistry*, *232*, 241–248.

Khalid, N. R., Ahmed, E., Hong, Z., Zhang, Y., Ullah, M., & Ahmed, M. (2013). Graphene modified Nd/TiO_2 photocatalyst for methyl orange degradation under visible light irradiation. *Ceramics International*, *39*(4), 3569–3575.

Khan, M. M., Adil, S. F., & Al-Mayouf, A. (2015). Metal oxides as photocatalysts. *Journal of Saudi Chemical Society*, *19*(5), 462–464.

Laxmi J. Tomar, Piyush J. Bhatt, R. k. D. and B. S. C. (2014). Effect of Preparation Method on Optical and Structural Properties of TiO_2/ZrO_2 Nanocomposite. *Journal of Nanotechnology & Advanced Materrials 33*(1), 27–33.

Lemlikchi, W., Sharrock, P., Fiallo, M., Nzihou, A., & Mecherri, M. (2014). Hydroxyapatite and Alizarin sulfonate ARS modeling interactions for textile dyes removal from wastewaters. *Procedia Engineering*, *83*, 378–385.

Li, C., Sun, Z., Xue, Y., Yao, G., & Zheng, S. (2016). A facile synthesis of g-C_3N_4/TiO_2 hybrid photocatalysts by sol – gel method and its enhanced photodegradation towards methylene blue under visible light. *Advanced Powder*

Technology, (January), 1–8.

Li, J., Yanli Liu, Li, H., & Chen, C. (2013). Improved photocatalytic activity of g-C_3N_4/TiO_2 composites prepared by a simple impregnation method. *Journal of Photochemistry and Photobiology A : Chemistry 253*, 16–21.

Li, X., Gu, J., Li, Y., Shi, J., Tang, Y., Wan, Y., & Shi, J. (2014). Promotion effects of SiO_2 or/and Al_2O_3 doped CeO_2/TiO_2 catalysts for selective catalytic reduction of NO by NH_3. *Journal of Hazadous Materials* 2–5.

Liao, L., & Duan, X. (2012). Graphene for radio Graphene is emerging as an attractive electronic material for future. *Materials Today*, *15*(7–8), 328–338.

Lin, H. Y., & Shih, C. Y. (2015). Efficient one-pot microwave-assisted hydrothermal synthesis of M (M = Cr, Ni, Cu, Nb) and nitrogen co-doped TiO_2 for hydrogen production by photocatalytic water splitting. *Journal of Molecular Catalysis A: Chemical*, *411*, 128–137.

Linnik, O., Shestopal, N., Smirnova, N., Eremenko, A., Korduban, O., Kandyba, V., … Mihailescu, I. N. (2015). Correlation between electronic structure and photocatalytic properties of non-metal doped TiO_2/ZrO_2 thin films obtained by pulsed laser deposition method. *Vaccum*, 8–13.

Liu, T., Li, B., Hao, Y., Han, F., Zhang, L., & Hu, L. (2015). Applied Catalysis B : Environmental A general method to diverse silver / mesoporous – metal – oxide nanocomposites with plasmon-enhanced photocatalytic activity. *"Applied Catalysis B, Environmental," 165*, 378–388.

López-ayala, S., Rincón, M. E., Alfaro, M. A. Q., Bandala, E. R., Rojas, M. A. M., & Castaño, V. M. (2015). Nanocrystalline titania xerogels doped by metal precursors in the photocatalytic degradation of 2 , 4-D sodium salts. *"Journal of Photochemistry & Photobiology, A: Chemistry," 311*, 166–175.

Ma, C., Zhou, J., Cui, Z., Wang, Y., & Zou, Z. (2016). In situ growth MoO_3 nanoflake on conjugated polymer: An advanced photocatalyst for hydrogen evolution from water solution under solar light. *Solar Energy Materials and Solar Cells*, *150*, 102–111.

Mainya, N. O., Tum, P., & Muthoka, T. M. (2015). Photodegradation and Adsorption of Methyl Orange and Methylene Blue Dyes on TiO_2. *International Journal of Science and Research (IJSR) 4*(4), 3185–3189.

Marschall, R., & Wang, L. (2013). Non-metal doping of transition metal oxides for visible-light photocatalysis. *Catalysis Today*. 25

Momeni, M. M., & Ghayeb, Y. (2016). Fabrication, characterization and photocatalytic properties of Au/TiO_2-WO_3 nanotubular composite synthesized by photo-assisted deposition and electrochemical anodizing methods. *Journal of Molecular Catalysis A: Chemical* 417, 107-115.

Nainani, R., Thakur, P., & Chaskar, M. (2012). Synthesis of Silver Doped TiO_2 Nanoparticles for the Improved Photocatalytic Degradation of Methyl Orange. *Journal of Materials Science and Engineering 2*(1), 52–58.

Ng, K. H., Lee, C. H., Khan, M. R., & Cheng, C. K. (2016). Photocatalytic degradation of recalcitrant POME waste by using silver doped titania: Photokinetics and scavenging studies. *Chemical Engineering Journal*, *286*, 282–290.

Nitoi, I., Oancea, P., Raileanu, M., Crisan, M., Constantin, L., & Cristea, I. (2015). UV-VIS photocatalytic degradation of nitrobenzene from water using heavy metal doped titania. *Journal of Industrial and Engineering Chemistry*, *21*, 677–682.

Nuengmatcha, P., Chanthai, S., Mahachai, R., & Oh, W. (2016). Journal of Environmental Chemical Engineering Visible light-driven photocatalytic degradation of rhodamine B and industrial dyes (texbrite BAC-L and texbrite NFW-L) by ZnO-graphene. *Biochemical Pharmacology*, *4*(2), 2170–2177.

Petcu, A. R., Lazar, C. A., Rogozea, E. A., Olteanu, L., Meghea, A., & Mihaly, M. (2015). Nonionic microemulsion systems applied for removal of ionic dyes mixtures from textile industry wastewaters. *Separation And Purification Technology*. 9-10

Ramacharyulu, P. V. R. K., Praveen Kumar, J., Prasad, G. K., Singh, B., Sreedhar, B., & Dwivedi, K. (2014). Sunlight assisted photocatalytic detoxification of sulfur mustard on vanadium ion doped titania nanocatalysts. *Journal of Molecular Catalysis A: Chemical*, *387*, 38–44.

Roy, H. G. (2013). Optical properties and photocatalytic activities of titania nanoflowers synthesized by microwave irradiation. *International Journal of Innovative Research in Science, Engineering and Technology*, *2*(6), 2175–2181.

Saranya, J., Ranjith, K. S., Saravanan, P., Mangalaraj, D., & Rajendra Kumar, R. T. (2014). Cobalt-doped cerium oxide nanoparticles: Enhanced photocatalytic activity under UV and visible light irradiation. *Materials Science in Semiconductor Processing*, *26*(1), 218–224.

Semeraro, P., Rizzi, V., Fini, P., Matera, S., Cosma, P., García, R., & Ferrándiz, M. (2015). Interaction between industrial textile dyes and cyclodextrins. *Dyes and Pigments*. 1-2

Shao, G. N., Engole, M., Imran, S. M., Jeong, S., & Taik, H. (2015). Applied Surface Science Sol – gel synthesis of photoactive kaolinite-titania : Effect of the preparation method and their photocatalytic properties. *Applied Surface Science*, *331*, 98–107.

Shtarev, D. S., Shtareva, A. V, Syuy, A. V, & Pereginiak, M. V. (2016). Optik Synthesis and photocatalytic properties of alkaline earth metals bismuthates – bismuth oxide compositions. *Optik - International Journal for Light and Electron Optics*, *127*(3), 1414–1420.

Siriwong, C., Wetchakun, N., Inceesungvorn, B., Channei, D., Samerjai, T., & Phanichphant, S. (2012). Doped-metal oxide nanoparticles for use as photocatalysts. *Progress in Crystal Growth and Characterization of Materials*, *58*(2–3), 145–163.

Stengl, V., Bakardjieva, S., Grygar, T. M., Bludská, J., & Kormunda, M. (2013). TiO_2-graphene oxide nanocomposite as advanced photocatalytic materials. *Chemistry Central Journal*, *7*(1), 41.

Stojadinović, S., Vasilić, R., Radić, N., Tadić, N., Stefanov, P., & Grbić, B. (2016). The formation of tungsten doped Al_2O_3/ZnO coatings on aluminum by plasma electrolytic oxidation and their application in photocatalysis. *Applied Surface Science*, 377, 37-43.

Su, C., Li, Y., He, Y., Liu, L., Wang, X., & Liu, L. (2015). Al_2O_3-doped for enhancing ethanol sensing properties of α-Fe_2O_3 nanotubes. *Materials Science in Semiconductor Processing*, *39*, 49–53.

Tang, C. (2013). Study of Photocatalytic Degradation of Methyl Orange on Different Morphologies of ZnO Catalysts. *Modern Research in Catalysts* 2, 19–24.

Tang, W., Qiu, K., Zhang, P., & Yuan, X. (2015). Synthesis and photocatalytic activity of ytterbium-doped titania/diatomite composite photocatalysts. *Applied Surface Science*, 3–5.

Tuan Vu, A., Tuan Nguyen, Q., Linh Bui, T. H., Cuong Tran, M., Phuong Dang, T., & Hoa Tran, T. K. (2010). Synthesis and characterization of TiO_2 photocatalyst doped by transition metal ions (Fe^{3+} , Cr^{3+} and V^{5+}). *Advances in Natural Sciences: Nanoscience and Nanotechnology*, *1*(1), 9-15.

Valentin, C. Di, & Pacchioni, G. (2013). Trends in non-metal doping of anatase TiO_2 : B , C , N and F, *206*, 12–18.

Vikas Somani. (2006). Alumina-aluminum titanate-titania nanocomposite : synthesis , sintering studies , assessment of bioactivity and its mechanical and electrical properties. University of Central Florida.

Wan, J., Sun, L., Liu, E., Fan, J., Hu, X., Pu, C., & Du, X. (2016). Novel UV–vis-driven photocatalysts of CeF_3/TiO_2 nano-sheet film with upconversion properties for enhanced photocatalytic activity. *Materials Letters*, *169*, 189–192.

Wang, W., Liu, Y., Sun, J., & Gao, L. (2016). Nitrogen and yttrium co-doped mesoporous titania photoanodes applied in DSSCs. *Journal of Alloys and Compounds*, *659*, 15–22.

Wang, Y., Xue, X., & Yang, H. (2014). Preparation and characterization of carbon or / and boron-doped titania nano-materials with antibacterial activity. *Ceramics International*, (4 ml), 1–5.

Yamjala, K., Subramania, M., & Rao, N. (2016). Methods for the analysis of azo dyes employed in food industry – A review. *Food Chemistry*, *192*, 813–824.

Yan, T., & Wei, G. (2014). Multiscale Analysis of the Interfacial Mechanical Behavior for Composite of Carbon Nanotube and α-Alumina. *Advances in Materials Science and Engineering*, 1–2.

Yang, G., Wang, T., Yang, B., Yan, Z., Ding, S., & Xiao, T. (2013). Enhanced visible-light of F-N co-doped TiO_2 nanocrystal via nonmetal impurity Ti^{3+} ions and oxygen vacancies. *Applied Surface Science*. 2-3

Yin, W. J., Chen, S., Yang, J. H., Gong, X. G., Yan, Y., & Wei, S. H. (2010). Effective band gap narrowing of anatase TiO_2 by strain along a soft crystal direction. *Applied Physics Letters*, *96*(22), 2.

Yong, D., Park, J., Kim, Y., Lee, M., & Cho, N. (2014). Effect of Nb doping on morphology , crystal structure , optical band gap energy of TiO_2 thin fi lms. *Current Applied Physics*, *14*(3), 421–427.

Yue, X., Jin, X., Wang, R., Ni, L., Jiang, S., Qiu, S., & Zhang, Z. (2016). Facile synthesis of metal-doped titania nanospheres with tunable size exhibiting highly efficient photoactivity for degradation. *Materials Chemistry and Physics*, 1–9.

Zhang, H. P., Luo, X. G., Lin, X. Y., Zhang, Y. P., Tang, P. P., Lu, X., & Tang, Y. (2015). Band structure of graphene modulated by Ti or N dopants and applications in gas sensoring. *Journal of Molecular Graphics and Modelling*, *61*, 224–230.

Zhang, H., Xu, P., Du, G., Chen, Z., Oh, K., Pan, D., & Jiao, Z. (2011). A Facile One-Step Synthesis of TiO_2/Graphene Composites for Photodegradation of Methyl Orange. *Journal of Molecular Graphics and Modellig 4*(3), 274–283.

Zhang, W., Xiao, X., Zheng, L., & Wan, C. (2015). Applied Surface Science Fabrication of TiO_2/MoS_2 @ zeolite photocatalyst and its photocatalytic activity for degradation of methyl orange under visible light. *Applied Surface Science*, *358*, 468–478.

Zhang, X., Li, D., Wan, J., & Yu, X. (2016). Processing Hydrothermal synthesis of TiO_2 nanosheets photoelectrocatalyst on Ti mesh for degradation of nor fl oxacin : Influence of pickling agents, *Materials Science in Semiconductor 43*, 47–54.

Zou, Y., Gong, Y., Lin, B., & Mellott, N. P. (2016). Photodegradation of methylene blue in the visible spectrum: An efficient W^{6+} ion doped anatase titania photocatalyst via a solvothermal method. *Vacuum*, *126*, 63–69.

APPENDIX A

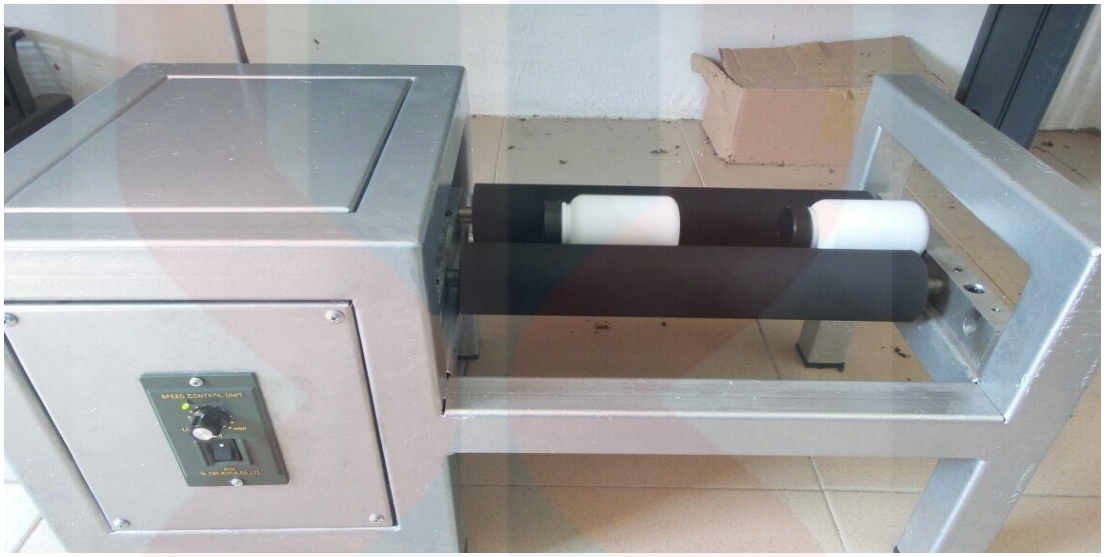

Figure A.1: TiO_2-Al_2O_3-graphene nanocomposites during ball milling process.

Figure A.2: TiO_2-Al_2O_3-graphene nanocomposites in autoclave after 24 h at 200°C

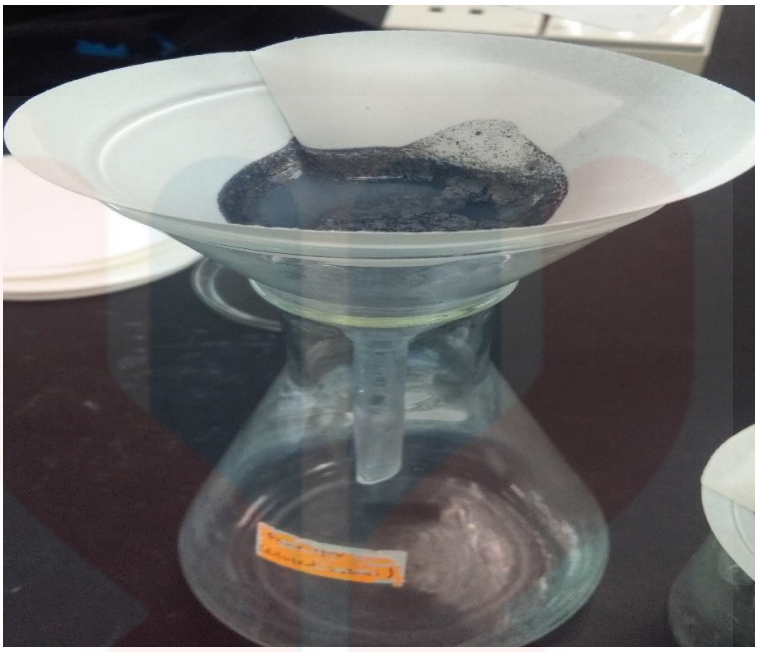

Figure A.3: TiO_2-Al_2O_3-graphene nanocomposites during filter process

Figure A.4: TiO_2-Al_2O_3-graphene after drying process

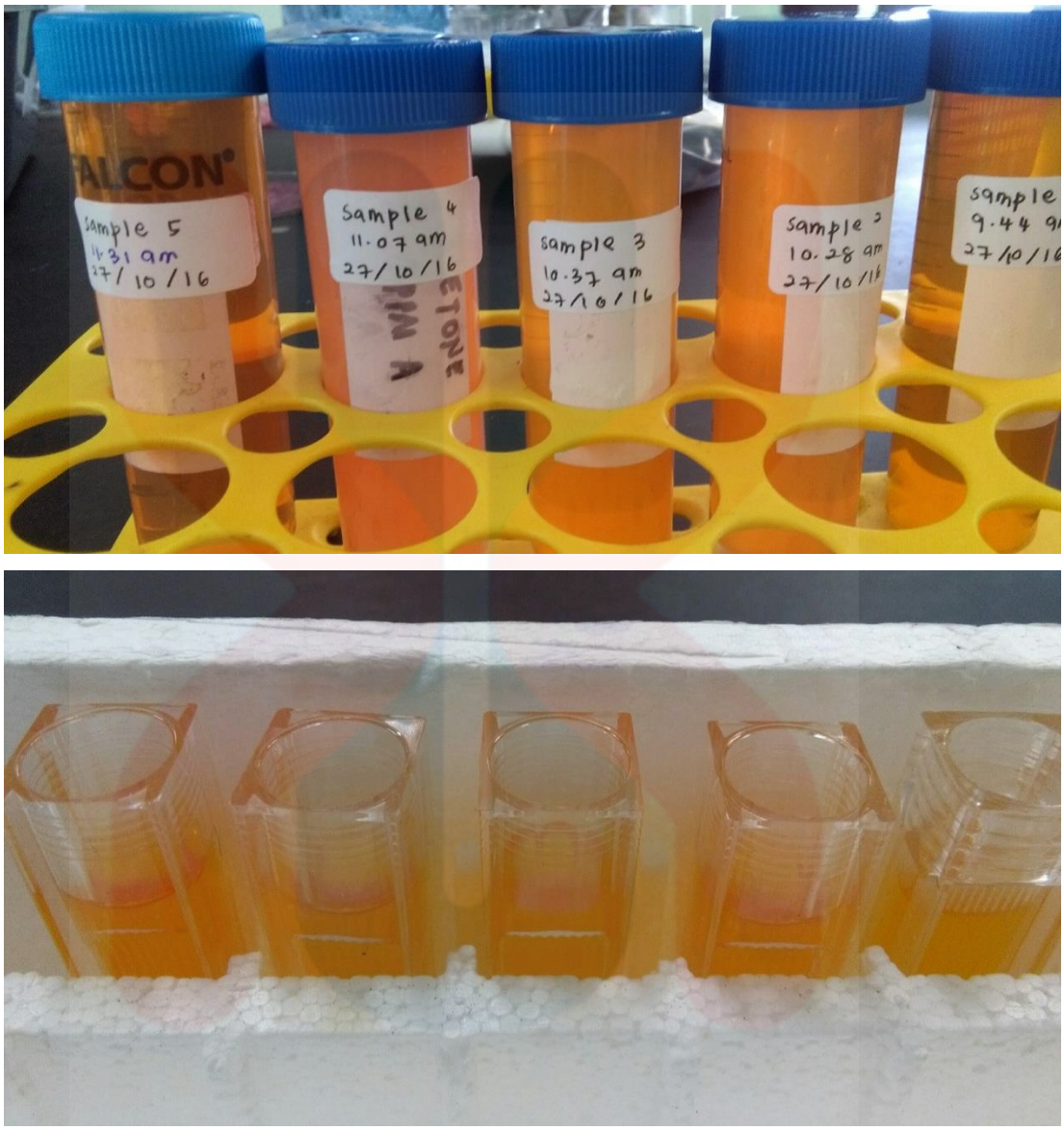

Figure A.5: Methyl orange solution

APPENDIX B

CALCULATIONS

B.1 Calculation of Percentage Absorbance of Methyl Orange

Example calculation are:

$$\text{Photocatalytic absorbance (\%)} = \left(\frac{Co - C}{Co}\right)$$

Eq.4

For TA60,

$$\text{Photocatalytic absorbance (\%)} = \left(\frac{1.896 - 1.282}{1.896}\right)$$

$$= 32.384\%$$

For TAG80,

$$\text{Photocatalytic absorbance (\%)} = \left(\frac{1.896 - 1.877}{1.896}\right)$$

$$= 1.002\%$$

For TAG70,

$$\text{Photocatalytic absorbance (\%)} = \left(\frac{1.896 - 1.740}{1.896}\right)$$

$$= 8.228\%$$

For TAG60,

$$\text{Photocatalytic absorbance (\%)} = \left(\frac{1.896 - 1.863}{1.896}\right)$$

$$= 1.741\%$$

For TAG50,

Photocatalytic absorbance (%) = $\left(\frac{1.896 - 1.331}{1.896}\right)$

= 29.8%

B.2 Calculation of Crystallite Size and Internal Strain using WH Method

The crystallite size and internal strain of TiO_2 can be calculated from

$$B_r \cos\theta = \left(\frac{k\lambda}{D}\right) + \eta \sin\theta \qquad \text{Eq. 1}$$

Example calculation for TiO_2 are: